Journal of proteome research

pubs.acs.org/jpr

Article

DIA-Based Proteome Profiling of Nasopharyngeal Swabs from COVID-19 Patients

Dong-Gi Mun, Patrick M. Vanderboom, Anil K. Madugundu, Kishore Garapati, Sandip Chavan, Jane A. Peterson, Mayank Saraswat, and Akhilesh Pandey*

Cite This: https://doi.org/10.1021/acs.jproteome.1c00506

Read Online

ACCESS | Metrics & More | Article Recommendations | Supporting Information

ABSTRACT: Since the recent outbreak of COVID-19, there have been intense efforts to understand viral pathogenesis and host immune response to combat SARS-CoV-2. It has become evident that different host alterations can be identified in SARS-CoV-2 infection based on whether infected cells, animal models or clinical samples are studied. Although nasopharyngeal swabs are routinely collected for SARS-CoV-2 detection by RT-PCR testing, host alterations in the nasopharynx at the proteomic level have not been systematically investigated. Thus, we sought to characterize the host response through global proteome profiling of nasopharyngeal swab specimens. A mass spectrometer combining trapped ion mobility spectrometry (TIMS) and high-resolution QTOF mass spectrometer with parallel accumulation-serial fragmentation (PASEF) was deployed for unbiased proteome profiling. First, deep proteome profiling of pooled nasopharyngeal swab samples was performed in the PASEF enabled DDA mode, which identified 7723 proteins that were then used to generate a spectral library. This approach provided peptide level evidence of five missing proteins for which MS/MS spectrum and mobilograms were validated with synthetic peptides. Subsequently, quantitative proteomic profiling was carried out for 90 individual nasopharyngeal swab samples (45 positive and 45 negative) in DIA combined with PASEF, termed as diaPASEF mode, which resulted in a total of 5023 protein identifications. Of these, 577 proteins were found to be upregulated in SARS-CoV-2 positive samples. Functional analysis of these upregulated proteins revealed alterations in several biological processes including innate immune response, viral protein assembly, and exocytosis. To the best of our knowledge, this study is the first to deploy diaPASEF for quantitative proteomic profiling of clinical samples and shows the feasibility of adopting such an approach to understand mechanisms and pathways altered in diseases.

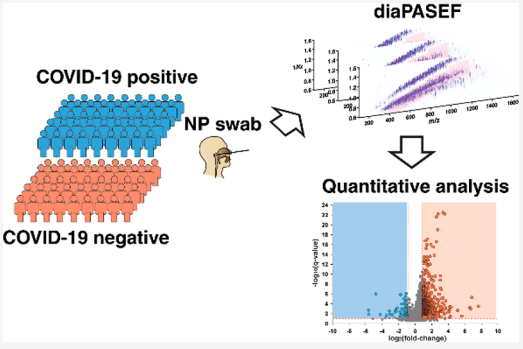

KEYWORDS: *diaPASEF, COVID-19, host response*

INTRODUCTION

Recent advances in data-independent acquisition (DIA), especially owing to the high-performance mass spectrometers and improved data analysis strategies, have enabled unbiased measurement of proteomes.[1−4] A major benefit of DIA compared to data-dependent acquisition (DDA)-based approaches is the reproducible measurements across runs, which allows application to large sample cohorts.[5] However, it is also understood that a major limitation of DIA is the complexity of MS/MS spectra that hinders accurate and sensitive peptide identification. Therefore, various strategies have been introduced to circumvent this issue in terms of data acquisition method, as well as data interpretation pipelines.[2] Recently, it was shown that addition of ion mobility separation could further increase the sensitivity of peptide identification by decreasing the complexity of MS/MS spectra. Further, coupling ion mobility separation to DIA through trapped ion mobility mass spectrometer (TIMS) has been suggested to reach nearly 100% ion sampling efficiency.[6] This new acquisition strategy, termed diaPASEF, incorporates the idea that there is correlation between peptide ion mass and ion mobility. Two TIMS configuration operating in parallel for ion accumulation and mobility separation combined with a quadrupole allow data acquisition of every mass window at the specific time, which overcomes a limitation of conventional DIA methods acquiring fragment ions from one isolation window. In addition, data interpretation utilizing ion mobility in addition to elution time and precursor window contributes to increased signal-to-noise ratios.

Severe acute respiratory syndrome coronavirus 2 (SARS-CoV-2) the causative organism of the COVID-19 pandemic,

Received: June 19, 2021

poses a substantial threat to human health. SARS-CoV-2 infection usually causes mild symptoms but hyperinflammatory immune response has been observed in a subset of patients with severe consequences such as acute respiratory distress syndrome.[7] Therefore, a number of studies to understand host response in infected cells, animal models, and clinical samples using genomics[8−11] and proteomics approaches[12−14] have been performed. Further, multi-omics analysis has revealed dysregulated molecules in the blood of COVID-19 patients.[15,16]

SARS-CoV-2 enters the body mainly through the nasal cavity, which is connects posteriorly to the pharynx, larynx and the lower respiratory tract. Located at the interface with the external environment, the nasopharynx plays a critical role as a first line of defense against pathogens.[17,18] SARS-CoV-2 enters cells in the respiratory tract by binding of its S protein to angiotensin-converting enzyme 2 (ACE2) on the host cell surface, followed by cleavage by serine protease TMPRSS2.[19,20] Given that the nasopharynx is the primary site of SARS-CoV-2 exposure, host proteome profiles of nasopharynx would provide the clue that can help understanding pathogenesis and discovering drug targets. The upper respiratory tract including the nasopharyngeal mucosa can be easily sampled using nasopharyngeal swabs (NP swabs), which are the standard sampling for diagnostic testing for COVID-19. In this regard, while several mass spectrometry-based studies have employed NP swabs for detection of viral peptides,[21−23] host proteome profiling of NP swabs has lagged behind[14] although it offers an attractive opportunity for studying the impact of SARS-CoV-2 on epithelial as well as immune cells.

In this study, we sought to characterize the proteome host response by analyzing NP swab specimens. Proteome profiles of 45 SARS-CoV-2 positive and 45 negative NP swab samples were acquired with diaPASEF mode. Data interpretation was performed by employing a spectral library generated specifically for this purpose from extensively fractionated samples prepared from pooled COVID-19 positive, as well as COVID-19 negative samples. Functional analysis demonstrated that innate immune responses were elevated in SARS-CoV-2 positive subjects, which includes IFN-mediated immune response and complement activation. In addition, processes related to viral life cycle were shown to be upregulated, such as endoplasmic reticulum (ER) to Golgi vesicle-mediated transport and exocytosis. To the best of our knowledge, this is the first use of diaPASEF on clinical samples to decipher the host response against SARS-CoV-2. We believe that the record of nasopharyngeal proteome would provide information for better understanding host response against SARS-CoV-2 infection and finally suggest potential therapeutic targets.

EXPERIMENTAL SECTION

Collection of NP Swab Specimens

NP swabs were obtained from samples submitted to the diagnostic clinical laboratory at Mayo Clinic in Rochester, Minnesota after approval from the Mayo Clinic Institutional Review Board. All swabs used in this study were inactivated at 70 °C for 30 min prior to further processing. In total, 45 SARS-CoV-2 positive and 45 negative NP swab samples were used in this study.

Protein Extraction and Digestion

NP swabs were collected in PBS. About 200 μL of PBS was taken for 67 samples and an additional amount (1 mL) was used from 23 samples to make pooled peptide samples that were used for generating a spectral library. Protein precipitation was performed by adding methanol (nine times by volume) and pelleted by centrifugation at 16 000*g* for 15 min. The precipitated proteins were reconstituted in 8 M urea in 50 mM TEAB (pH 8.0) and protein concentration was measured using BCA assay (Thermo, 23227). Protein lysates were reduced using 10 mM dithiothreitol for 30 min, followed by alkylation with 40 mM iodoacetamide for 30 min. Protein digestion was carried out using trypsin (Promega, V5111) overnight at 37 °C (1:50 enzyme to protein ratio). The peptides were desalted using C_{18} stage tips (Glygen, TT2C18) or in-house tip packed with C_{18} disk (3M, Empore). iRT peptides (Biognosys, *Ki*-3002-1) were injected for all samples analyzed in this study.

Generation of Spectral Library from Pooled Samples with PASEF-DDA

Peptides from pooled samples (∼1.6 mg) were loaded on a Xbridge column (4.6 mm × 50 cm × 3.5 μm, Waters, Milford, MA) and separated using Dionex Ultimate 3000 liquid chromatography system (Thermo Scientific, Waltham, MA). Mobile phase A was composed of 20 mM ammonium formate in water (pH 8.5), and mobile phase B was composed of 20 mM ammonium formate in 80% ACN (pH 8.5). Two hours gradient was applied from 2% to 40% of sol B and 96 fractions were collected at every 75 s. The fractions were concatenated into 24 fractions and ∼5 μg of peptides of each fraction were analyzed in DDA mode to generate a spectral library. nanoElute liquid chromatography system (Bruker Daltonics, Bremen, Germany) was operated with two column separation mode connected to an analytical column (25 cm × 75 μm, 1.6 μm C_{18}, IonOpticks, AUR2-25075C18A-CSI) and a trap column (2 cm × 100 μm, Acclaim PepMap100, Thermo Fisher Scientific). The analytical column was kept at 50 °C. Solvent A was 0.1% formic acid in water, and solvent B was prepared with 0.1% formic acid in acetonitrile. The peptides were separated over 130 min at 300 nL/min using the following gradients: from 3% to 35% sol B in 120 min, from 35% to 80% sol B in 5 min, maintaining at 80% for 10 min and equilibrating 3% sol B for 5 min. Eluted peptide were analyzed on timsTOF Pro (Bruker Daltonics, Bremen, Germany) in the PASEF-DDA mode. TIMS was enabled with 100 ms of ramp time and 100% duty cycle. Ions with ion mobility from 0.6 to 1.6 V s cm^{-2} were monitored. MS/MS data were acquired with 10 PASEF MS/MS scans per cycle. Isolation width was set to 2 m/z for m/z < 700 and 3 m/z for m/z > 800. Collision energy was increased stepwise from 20 to 59 eV as a function of increasing ion mobility from 0.6 to 1.6 V s cm^{-2}. MS and MS/MS spectra were acquired from m/z 100 to 1700.

Acquisition of diaPASEF Data

Individual 90 samples (45 positive and 45 negative) were analyzed in the diaPASEF mode by injecting 1 μg of peptide mixture. The same separation conditions were used as in DDA experiment. The mass spectrometer was operated in the DIA mode controlled with text file containing all parameters for diaPASEF experiment (Supplementary Table 1). The isolation width was set as 25 m/z and precursor ions of 400−1,200 m/z and ion mobility of 0.69−1.47 V s cm^{-2} were monitored with 64 windows.[6] Collision energy was ramped linearly from 20 to 59 eV as was done for the PASEF-DDA experiments.

https://doi.org/10.1021/acs.jproteome.1c00506
J. Proteome Res. XXXX, XXX, XXX−XXX

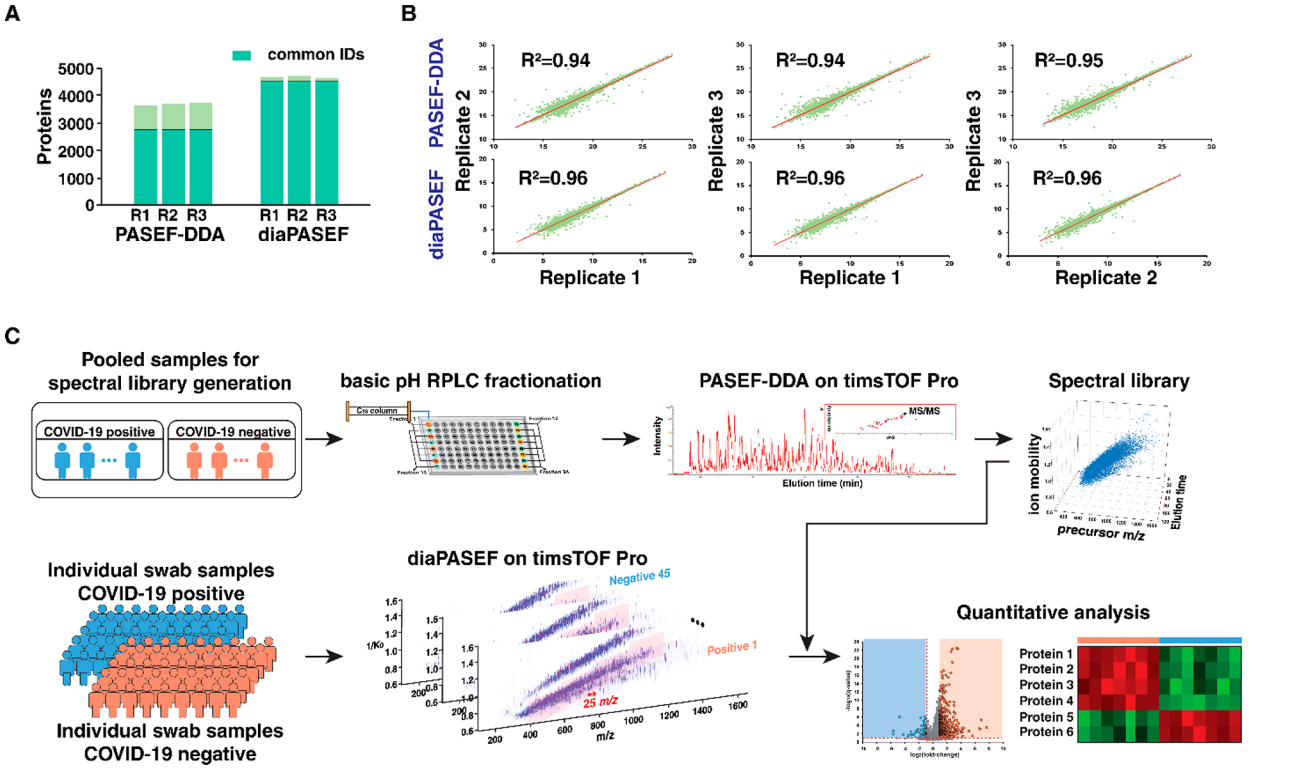

Figure 1. Performance evaluation and design of the study. (A) Bar charts of the number of protein groups from triplicates of PASEF-DDA and diaPASEF experiments. All LC-MS/MS experiments were acquired with the same parameters as described under the Methods section by injecting ~1 μg of peptides from Jurkat cells. (B) Correlation of protein abundance from triplicate PASEF-DDA and diaPASEF analyses is shown. Quantitative values of proteins in PASEF-DDA and diaPASEF were obtained through MaxQuant and Spectronaut, respectively. (C) Overall workflow for DIA-based proteome profiling. The nasopharyngeal swab samples were processed and analyzed using the diaPASEF mode on timsTOF Pro mass spectrometer. The spectral library generated from PASEF-DDA data acquired from pooled samples was used for DIA interpretation through Spectronaut.

Data Analysis

PASEF-DDA data from 48 fractionated samples were loaded to Spectronaut 14 (version 14.10.201222.47784, Biognosys). A spectral library was generated using Pulsar in Spectronaut 14 under the default settings. Combined protein database of UniProt human database (20 501 entries), SARS-CoV-2 proteins, SARS-CoV proteins and common coronaviruses proteins (OC43, HKU1, NL63, and L229E) were used for protein identification. A maximum of two missed cleavages were considered with trypsin as the enzyme. Carbamidomethylation of cysteine was set as a fixed modification. Protein N-terminal acetylation and oxidation of methionine were set as variable modifications. The generated spectral library can be found in Supplemental Table 2. The same data were searched against neXtProt database using Andromeda in MaxQuant suite for evaluating iBAQ values and missing proteins under the same search parameters as described above. diaPASEF data were analyzed using Spectronaut 14 against the spectral library using the BGS factory default settings. The identifications were filtered at an FDR of 1% at both peptide and protein levels. Differentially expressed proteins ((|fold-change| > 2 and adjusted p-value <0.05) reported from Spectronaut were used as input to Ingenuity Pathway Analysis software (Qiagen, Germantown, MD) for further functional analyses. The heatmap was generated using MetaboAnalyst 5.0 (https://www.metaboanalyst.ca/). Protein abundance was log transformed and scaled with auto scaling setting. Protein−protein interactions were evaluated with STRING (version 11.0).[24]

Peptide Synthesis

The peptides were synthesized using standard FMOC chemistry on a MultiPep RSi (CEM Corp. Matthews, NC) multiple peptide synthesizer retrofitted with a 384-well filter plate. The starting resin for peptides were FMOC-Arg(pbf) Wang resin or FMOC-Lys(Boc) Wang resin (Novabiochem, Burlington, MA). The peptides were cleaved for 2 h at room temperature and, then, centrifuged onto a receiving plate for 2 min at 1000 rpm. Cleavage cocktail was trifluoroacetic acid, water, triisopropyl silane, and 3,6-dioxa-1,8-octanedithiol (92.5/2.5/2.5/2.5 v/v/v/v). Peptides were washed with dichloromethane and added to the volume of cleavage cocktail in the receiving plate. Cold MTBE was added to precipitate the peptides, and then, the plate was placed at −20 °C for 1 h. The precipitates were centrifuged for 2 min at 1000 rpm and then placed in a hood to dry overnight.

Data Availability

The DIA mass spectrometry data have been deposited to the ProteomeXchange Consortium via the PRIDE partner repository[25] with the data set identifier PXD025277. The spectral library used in this study can be found in the Supplementary Data.

https://doi.org/10.1021/acs.jproteome.1c00506
J. Proteome Res. XXXX, XXX, XXX−XXX

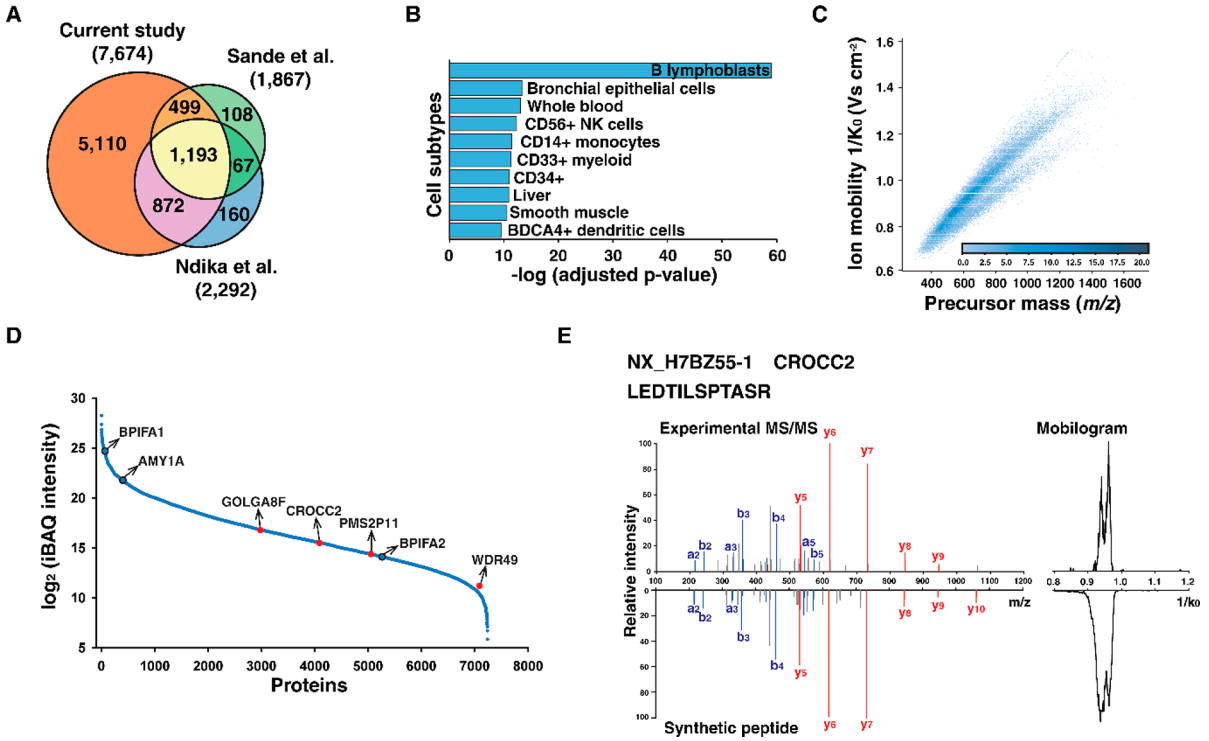

Figure 2. Generation of a proteome catalog of the nasopharynx. (A) Comparison of nasopharynx proteomes with previous proteomics studies from NP swab or brush samples. (B) Cellular deduced subtypes of proteins identified in PASEF-DDA experiments. (C) Density distribution of precursor mass and ion mobility values of 102 392 precursors contained in the spectral library. (D) Distribution of iBAQ intensity of the identified proteins. The representative proteins known to be expressed in nasopharynx are marked as empty black circle. The missing proteins are marked as red circles. (E) MS/MS spectrum and mobilogram of experimental and synthetic peptide LEDTILSPTASR derived from the missing protein, CROCC2.

RESULTS AND DISCUSSION

Design of the Study for Comprehensive Quantitative Proteome Profiling

A major shortcoming of the DDA approach is the lack of reproducible measurements across samples mainly because of the stochastic nature of precursor ion sampling during MS/MS analysis.[26] In contrast, the DIA approach ensures fragmentation of all precursor ions within any predetermined isolation window to significantly improve the reproducibility of proteomic measurements.[5] We deployed the timsTOF Pro mass spectrometer which supports PASEF mode coupled to DIA for our studies. The performance of DDA and DIA operated in PASEF mode was evaluated by injecting peptide digests of cultured Jurkat cells. As the effect of mass spectrometric parameters on protein identification has been investigated elsewhere,[27,28] we adopted the optimized settings for DDA and DIA experiments such as ion accumulation time, number of PASEF scans and size of the isolation window. The acquired PASEF-DDA data were then analyzed using Andromeda search engine within MaxQuant suite. In total, 4747 proteins were identified from triplicate runs with 2721 proteins (57%) repeatedly detected from all DDA experiments. In contrast, the same 4490 (94%) proteins were identified in each of the three DIA experiments (Figure 1A). Further, we observed highly reproducible quantitation between experiments. Correlation between diaPASEF experiments was slightly greater than that observed in PASEF-DDA experiments confirming reproducibility as a major benefit of DIA, which is highly desirable for large-scale analyses (Figure 1B).

We previously analyzed NP swabs to develop a mass-spectrometry-based assay for detecting viral antigens.[29] In our experiments aimed at detecting viral antigens, we observed several expected proteins related to interferon (IFN) mediated antiviral responses. This motivated us to investigate the host response against SARS-CoV-2 infection more systematically using a larger set of NP swab samples and a label-free approach. To accomplish this, we collected NP swabs from subjects who underwent RT-PCR-based molecular testing for diagnosis of COVID-19 infection and decided to perform diaPASEF-based analysis of individual samples for quantitative proteome profiling.

The overall workflow of proteome profiling of NP swabs is described in Figure 1C. We collected SARS-CoV-2 positive and negative NP swab specimens as determined from RT-PCR-based diagnostic testing. In RT-PCR test, the amount of SARS-CoV-2 RNA is estimated by cycle threshold (Ct) value which is inversely proportional to the viral loads. The median Ct value of positive samples in this study was 22.4 (range = 15.4−33.8). After protein lysis and digestion of NP swabs stored in PBS, equal amounts of peptides were used for proteomic profiling in the diaPASEF mode. Precursor ions spanning 400 to 1200 m/z with ion mobility from 0.69 to 1.47 V s cm^{-2} were monitored with 25 m/z isolation width. Sequential TIMS devices operating in parallel for ions accumulation and mobility separation coupled to mobility separation synchronized quadrupole allow nearly 100% sampling of precursor ion current in DIA mode. DIA data contain fragment ions of all precursor ions over the entire duration of elution. As spectral library with ion mobility information is essential for analyzing diaPASEF data, we generated two sets of sample pools—SARS-CoV-2 positive and negative samples. The pooled samples were separated into 24

https://doi.org/10.1021/acs.jproteome.1c00506
J. Proteome Res. XXXX, XXX, XXX−XXX

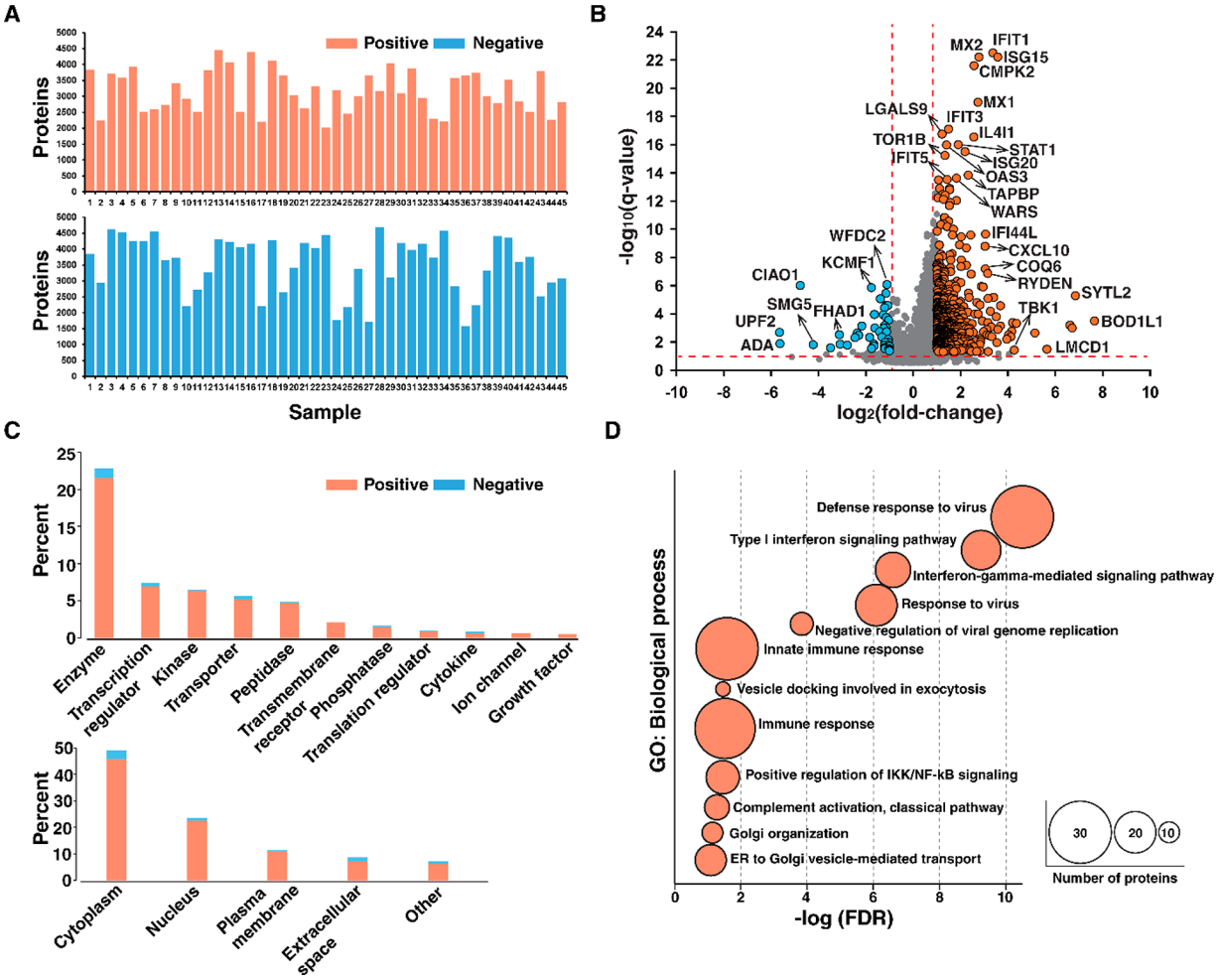

Figure 3. Quantitative analysis using diaPASEF (A) Bar charts of the number of proteins acquired from diaPASEF experimental analysis of 45 SARS-CoV-2 positive and 45 negative samples. (B) Volcano plot describing protein expression changes between positive and negative samples. (C) Bar charts displaying type of molecules and subcellular localization for differentially expressed proteins. (D) Gene ontology analysis of upregulated proteins. Biological processes are shown ordered according to the false discovery rate from DAVID (FDR < 0.05). The size of circle denotes the number of proteins associated with each biological process.

fractions by offline basic-pH RPLC fractionation. Each fraction (in total, 48 fractions) was analyzed in PASEF-DDA mode and subjected to protein database search to generate spectral library. Protein identification and quantitation of features of diaPASEF were obtained using Spectronaut against the generated spectral library.

Generating a Comprehensive Protein Catalog of the Nasopharynx with PASEF-DDA

PASEF-DDA data from fractionated samples were analyzed using Pulsar in Spectronaut which resulted in identification of 102 392 peptides corresponding to 7723 protein groups, which was then assembled as a spectral library. We assessed the comprehensiveness of the spectral library by comparing it with the previous proteome profiling studies of the nasopharynx (Figure 2A). There are a few studies performing proteome profiling of nasopharynx with swab or brush samples. Sande et al. identified 1875 proteins from NP swabs of 84 children with and without respiratory syncytial virus infection.[30] Ndika et al. performed proteome profiling of NP brushes of allergic rhinitis patients and controls, which resulted in 3207 proteins from 120 LC-MS/MS runs.[31] We, further, compared profiled proteome of nasopharynx from three studies at the gene level. This comparison showed most molecules detected in previous studies were covered by our studies. In addition, we identified 5110 genes that were missed previously. This confirms that our study provided the most extensive protein catalog from nasopharynx collected with NP swabs thus far.

The nasopharyngeal swab samples contain a heterogeneous mixture of immune and epithelial cells. This was supported by a cell subtype analysis using Enrichr[32] (Figure 2B). Immune cell subtypes including B lymphoblasts and NK cells were strongly enriched with immune cell-specific markers such as CD2, CD14, CD38, and granzyme B. Epithelial cells were also shown as the major cell subtype along with epithelial cell-specific markers including CDH1 and CLDN3.

We generated a spectral library with these comprehensive protein catalogs including information on elution time, ion mobility and fragment ions of peptides. Precursor ion masses ranged from 300 to 1700 m/z and ion mobility from 0.6 to 1.6 V s cm^{-2} (Figure 2C). We next evaluated the depth of the proteome through intensity-based absolute quantification (iBAQ) values.[33] The same data were searched against neXtProt database using Andromeda in MaxQuant and 7,243 protein groups were identified along with their iBAQ values. The protein abundance spanned 6 orders of magnitude of dynamic range (Figure 2D). The protein with the lowest

https://doi.org/10.1021/acs.jproteome.1c00506
J. Proteome Res. XXXX, XXX, XXX−XXX

expression was lymphocyte antigen 75 (LY75) while the most abundant protein was immunoglobulin kappa constant chain (IGKC). We could confidently detect several well characterized nasopharynx-specific proteins, such as BPIFA1/2 and AMY1A.

To further utilize the extensive protein profiles, we also mapped the identified proteins to the "missing protein" list from the neXtProt database.[34] Notably, five identified proteins (GOLGA8F, CROCC2, HSP90AA4P, PMS2P11, and WDR49) were labeled as missing protein. Of these, WDR49 was in the protein existence (PE) 2 (evidence only at the transcript level) category while the remaining four proteins were included in the PE5 (uncertain or dubious) category. Validation of the identification was carried out using synthetic peptides. MS/MS spectrum and mobilogram of peptide LEDTILSPTASR from protein CROCC2 provide a confident identification (Figure 2E). Interestingly, the evidence of CROCC2 was reported in Human Protein Atlas with high expression in nasopharynx and lung based on immunohistochemistry. In this study, we further provide the peptide evidence with experimental MS/MS spectrum and ion mobility values.

Proinflammatory cytokines are expected to be induced by innate immune cells against viral infection. We compared proteins consisting of the spectral library with a list of 255 cytokines, chemokines, and their receptors (https://www.immport.org/). Although several CXC chemokines (CXCL1, CXCL5, CXCL6, CXCL8, CXCL10, and CXCL17) and interleukins (IL16, IL18, IL19, and IL33) were identified and included in the spectral library, most cytokines were not detected through PASEF-DDA runs even with offline fractionation. This is mainly because of the low abundance of cytokines, which is still beyond the limit of detection of mass spectrometers. Further studies are required using complementary detection techniques such as proximity extension assays.[35]

Quantitative Analysis with diaPASEF of Individual Nasopharyngeal Swabs

Unbiased measurement of proteome for individual SARS-CoV-2 positive and negative NP swab samples were performed by injecting the same amount of peptide (i.e., 1 μg) with diaPASEF mode using an isolation window of 25 m/z. Spectronaut was used for protein identification using the spectral library that we generated. We detected a total of 79 703 peptides corresponding to 5023 protein groups and, on average, 3387 protein groups per sample (Figure 3A). Among them, 3496 proteins (71%) were shared across ≥45 samples and ∼15% of proteins (660 proteins) were shared across all 90 samples (Supplemental Figure 1A). The variation in the number of proteins was mainly due to biological variation and sampling across the NP swabs.

Protein abundance values were obtained from Spectronaut which enabled consideration of ion mobility during data extraction. Proteins quantified in only one sample of SARS-CoV-2 positive or negative group were excluded, and the resultant 4943 proteins were used for the further analysis. Among 4943 proteins 577 proteins were upregulated, and 46 proteins were downregulated (|fold-change| > 2 and adjusted p-value < 0.05) in SARS-CoV-2 positive samples (Figure 3B, Supplemental Table 3). As it was expected that IFN stimulated genes would be upregulated in SARS-CoV-2 positive subjects, we mapped upregulated proteins onto a web-based database of IFN regulated genes, Interferome.[36] This resulted in 432 proteins related to IFN regulated genes including IFIT1, IFIT2, IFIT3, IFIT5, ISG15, ISG20, MX1, MX2, OAS1, and OAS3. We also observed elevated expression levels of alarmin S100A8/A9, which is recently reported overexpression in SARS-CoV-2 infected models and COVID-19 patients.[10,37]

Differentially expressed proteins were categorized based on their function and subcellular localization through ingenuity pathway analysis (IPA). This analysis revealed that they belonged to various classes of molecules with 141 enzymes, 46 transcription regulators and 40 kinases from various cellular compartments mainly the cytoplasm (Figure 3C, Supplemental Table 3). Many kinases (39 molecules) were upregulated in COVID-19 positive samples including protein TBK1, CMPK2, and TAOK3. TANK binding kinase 1 (TBK1) is a well-characterized molecule that phosphorylates interferon regulatory factor 3 (IRF-3) in type I IFN signaling pathway. It has been reported that TBK1 acts as a core kinase in the innate immune response[38,39] and several studies have demonstrated that SARS-CoV-2 nonstructural protein 6 and 13 inhibit TBK1.[40,41] Cytidine/uridine monophosphate kinase 2 (CMPK2) was reported as an ISG that restricts HIV,[42] but less studied in SARS-CoV-2 related studies, which requires further investigation in the future.

Next, we performed gene ontology-based enrichment analysis of biological processes for upregulated proteins using DAVID.[43] This analysis revealed a significant enrichment of proteins associated with the innate immune response to viral infection including type I IFN and IFN-gamma-mediated signaling pathway (Figure 3D). Canonical pathways related to the innate immune response such as IFN signaling, activation of IRF by cytosolic pattern recognition receptors and increase cytokines/chemokines in the pathogenesis of influenza were again enriched in the IPA analysis (Supplemental Figure 1B). Although enrichment was not significant with FDR > 0.1, we observed several proteins (SERPINB10, BNIP3L, BCL2L1, and HMGA2) related to negative regulation of apoptotic process. Other proteins include proteins, such as WFDC2 and AGR3, which are known to be expressed in respiratory tract and are associated with immune response[44,45] although their exact role in SARS-CoV-2 is currently unknown.

There have been several studies to detect virus-derived peptides from NP swabs using mass spectrometry. We had previously observed a robust signal in a DDA experiment from a nucleocapsid-derived peptide, AYNVTQAFGR, which led us to evaluate the possibility of detecting it in a DIA experiment. Indeed, this peptide was detected in 23 positive samples with a confident MS/MS spectrum (Supplemental Figure 2A). The linear regression analysis between RT-PCR Ct and peak area showed a positive correlation with R^2 of 0.32 (Supplemental Figure 2B). This analysis describes the potential of a DIA-based approach recording all precursor ions in an unbiased fashion, which enables the reanalysis of the data in the future with different hypotheses including identification of peptides with coding mutations or with PTMs dysregulated by SARS-CoV-2 infection.

Elevated Innate Immune Response along with Expression of Various ISGs

We found a robust increase in the innate immune response against viral infection (Figure 3D and Supplemental Figure 1B). The innate IFN response pathway is one of the first lines of defense against viral infection. Upon viral infection, the host

https://doi.org/10.1021/acs.jproteome.1c00506
J. Proteome Res. XXXX, XXX, XXX−XXX

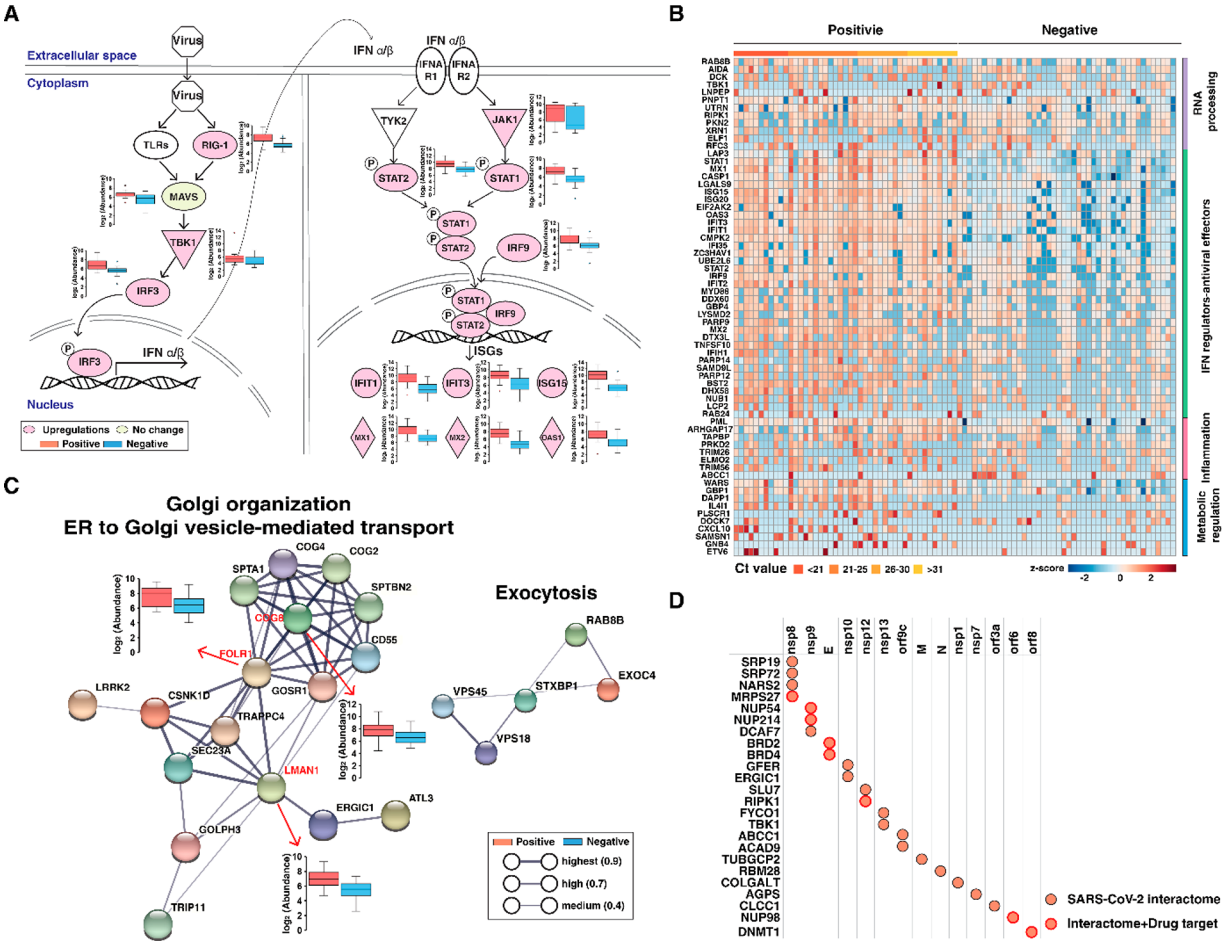

Figure 4. Functional analysis of upregulated proteins in SARS-CoV-2 positive subjects. (A) Representative canonical pathway elevated in positive samples. RIG-I-like receptors (RLRs) and Toll-like receptors (TLRs) mediated IFN-α/β production and downstream interferon signaling pathway are depicted. Box plots of selected proteins are shown. (B) Heatmap of 64 ISGs across 90 samples classified based on their function of RNA process, IFN regulators-antiviral effectors, inflammation, and metabolic regulation. (C) Protein−protein interactions of molecules related to Golgi organization, ER to Golgi vesicle-mediated transport and exocytosis. Box plots of proteins COG8, FOLR1, LMAN1 are shown. (D) Upregulated proteins that are known to interact with SARS-CoV-2.

pattern recognition receptors (PRRs) including retinoic acid-inducible gene I (RIG-I)-like receptors (RLRs) and Toll-like receptors (TLRs) recognize viral pathogen-associated molecular patterns (PAMPs).[46] Viral recognition triggers interaction of the caspase activation and recruitment domain (CARD) with the mitochondrial antiviral adaptor protein (MAVS). The activation of MAVS initiates downstream signaling, activating nuclear factor kB (NF-κB) and TANK binding kinase 1 (TBK1). These proteins phosphorylate interferon regulatory factor 3 (IRF-3) leading to nuclear translocation, and expression of type I IFN (IFN-I). Secreted IFN-I activates Janus kinase 1 (JAK1) and tyrosine kinase 2 (TYK2), which phosphorylate signal transducer and activator of transcription proteins (STAT1/2). Phosphorylated STAT1 and STAT2 form a heterodimer followed by association with interferon regulatory factor 9 (IRF9) to form ISGF3. This complex enters the nucleus and initiates expression of hundreds of ISGs. We observed a robust elevated protein expression of molecules associated with above-mentioned IFN signaling pathway (Figure 4A). Overexpression of proteins involved in IFN-mediated antiviral response is in agreement with previous studies on infected cells[12] bronchoalveolar lavage fluid,[9] and urine of COVID-19 patients.[47]

We further sought to classify the identified ISGs by their function and overlaid the proteins identified in this study on a list of 628 previously characterized ISGs.[48] In all, 65 proteins identified in this study were found in the list of characterized ISGs. Among the 65 ISGs identified in this data set, we found 35 classified as IFN mediators/antiviral effectors (Figure 4B). Interestingly, PARP9, PARP12, and PARP14 were among the 35 IFN mediators/antiviral effectors. PARP12 was previously shown to suppress zika virus infection in A549 cells by mediating ADP-ribosylation and subsequent proteasomal degradation of NS1 and NS3 nonstructural proteins.[49] We provide the resource of modulated ISGs that could be further investigated for improved understandings of host response related to antiviral activity against SARS-CoV-2.

In addition to the proteins that were described in the canonical pathway of IFN signaling (Figure 4A), we observed an interaction among upregulated proteins involved in functions such as inflammatory response and immunological diseases based on the network generated by IPA (Supplementary Figure 3). For example, we observed an upregulation of EIF2AK2 and RIPK1 kinases. EIF2AK2, also known as protein kinase R, acts as an antiviral protein that prevents viral replication by phosphorylating the initiation factor eIF2α. Receptor interacting protein kinase 1 (RIPK1) is a key

https://doi.org/10.1021/acs.jproteome.1c00506
J. Proteome Res. XXXX, XXX, XXX−XXX

molecule controlling cell death and inflammation.[50] To the best of our knowledge, this is the first report describing the upregulation of these molecules at the protein level in SARS-CoV-2 infected clinical samples.

Further, we observed complement activation through classical pathway with association of proteins, such as C3, C4A, C4BPB, and CD55 (Figure 3D, Supplemental Figure 3B). Complement system is known as a part of the innate immune response helping combat various infections.[51] Recently, overwhelming complement activation has been reported to play a role in respiratory failure and end-organ failure in COVID-19 patients.[52] Although we found relatively high expression level of C3, C4A, and CD55 in several samples, we could not evaluate the clinical significance of this observation as one of the limitations of this study was lack of corresponding clinical information on patients, such as disease status and severity. Our analysis was informed by the viral load in samples determined by RT-PCR, but we did not observe a significant correlation between viral load and protein expression levels of altered proteins.

Signatures of Active Viral Replication

In addition to antiviral immune responses, functional enrichment analysis revealed other biological processes related to viral replication, such as vesicle docking involved in exocytosis and endoplasmic reticulum (ER) to Golgi vesicle-mediated transport (Figure 3D). SARS-CoV-2 follows the general mechanism of viral infection—delivering RNA into the cell, followed by replication and subsequent release from the cell. In this context, it was expected that exocytosis pathway would be dominant in the SARS-CoV-2 positive subjects. We found seven upregulated proteins (VPS18/45, STXBP1, PLEK, EXOC4, RAB8B, and SYTL2) associated with the vesicle docking process in exocytosis. Similarly, elevated expression of ER to Golgi vesicle-mediated transport and Golgi organization process was altered, as viral replication and assembly utilize structural support from the ER-to-Golgi compartment, where different steps of the viral life cycle including replication and assembly take place.[53] This is in agreement with other reports that SARS-CoV-2 hijacks the early secretory pathway, including the ER, ER−Golgi intermediate compartment, and Golgi.[54]

Because most of the identified proteins related to ER or Golgi have not been reported in SARS-CoV-2 studies, we evaluated the protein−protein interaction (PPI) network of each process to enumerate molecules playing a pivotal role in each process. PPI network was built using STRING (version 11.0) under the confidence score ≥0.4 (Figure 4C). Protein LMAN1, COG8, and FOLR1 were shown to be the molecules with higher interaction in ER/Golgi related process. LMAN1 also known as ERGIC53 is a cargo receptor that was known to be associated with transporting glycoproteins in the early exocytotic pathway. It was demonstrated that LMAN1 is essential for viral life cycle and noninfectious viral particles are generated with loss of LMAN1.[55] COG8 is one of the members of the conserved oligomeric Golgi (COG) complex and is involved in intracellular membrane trafficking. Recently, it was reported that COG complex proteins facilitate entry and egress of orthopoxvirus, which suggested its potential as a therapeutic target intervening viral transport pathway.[56] Folate receptor 1 (FOLR1) has been reported to be upregulated in several cancers,[57] but it is seldom studied in viral research. Here, we provide evidence of elevated protein expression of LMAN1, COG complex including COG8 and FOLR1 in clinical samples of COVID-19 patients. The role of these proteins during SARS-CoV-2 infection and the interaction between SARS-CoV-2 are not clear and require further investigations to elucidate their exact roles.

To investigate if proteins interacting with SARS-CoV-2 could be potential therapeutic drug targets, we further evaluated if the differentially expressed proteins in our study interacted with viral protein by comparing our data set to previously reported SARS-CoV-2 interactome data obtained from infected cells.[58] Notably, we observed that 24 upregulated proteins from our data have been reported as interacting proteins with SARS-CoV-2 (Figure 4D). Among them, several proteins—MRPS27, NUP54/214, BRD2/4, RIPK1, NUP98, and DNMT1—have approved drugs that are known to inhibit these proteins, which could be investigated further using SARS-CoV-2 infection-based model systems. In any case, this is the first demonstration of elevated expression levels of these proteins in SARS-CoV-2 infected clinical sample and further functional analysis will be required to pursue them as potential targets in any therapeutic strategy.

CONCLUSIONS

In this study, we have demonstrated that comprehensive proteomic profiling of clinical samples using the diaPASEF approach could help decipher host response in response to SARS-CoV-2 infection. The data reveal activation of several biological processes including innate immune response (IFN signaling pathways and complement activation), as well as virus replication (exocytosis and ER/Golgi transport) in SARS-CoV-2 positive subjects. In addition to several proteins that have previously been shown to be regulated in SARS-CoV-2 infection, we discovered additional novel proteins to be altered, which will require further detailed and mechanistic studies. We believe that the proteomic profiles presented in this study could be exploited as the resource for mining potential drug targets, as well as understanding the response of host in COVID-19 infection.

ASSOCIATED CONTENT

Supporting Information

The Supporting Information is available free of charge at https://pubs.acs.org/doi/10.1021/acs.jproteome.1c00506.

Distribution of protein identified in multiple samples and enriched canonical pathways, representative example of detected viral peptide AYNVTQAFGR, and the top scoring networks in IPA (PDF)

Mass spectrometry settings of diaPASEF experiment (XLSX)

Spectral library used for interpretation of diaPASEF data (XLSX)

List of proteins quantified from 90 diaPASEF experiments (XLSX)

AUTHOR INFORMATION

Corresponding Author

Akhilesh Pandey − *Department of Laboratory Medicine and Pathology, Mayo Clinic, Rochester, Minnesota 55905, United States; Center for Molecular Medicine, National Institute of Mental Health and Neurosciences, Bangalore 560029 Karnataka, India; Center for Individualized Medicine, Mayo*

https://doi.org/10.1021/acs.jproteome.1c00506
J. Proteome Res. XXXX, XXX, XXX−XXX

Clinic, Rochester, Minnesota 55905, United States; orcid.org/0000-0001-9943-6127; Phone: 507-293-9564; Email: pandey.akhilesh@mayo.edu

Authors

Dong-Gi Mun − *Department of Laboratory Medicine and Pathology, Mayo Clinic, Rochester, Minnesota 55905, United States*

Patrick M. Vanderboom − *Department of Laboratory Medicine and Pathology, Mayo Clinic, Rochester, Minnesota 55905, United States*

Anil K. Madugundu − *Department of Laboratory Medicine and Pathology, Mayo Clinic, Rochester, Minnesota 55905, United States; Center for Molecular Medicine, National Institute of Mental Health and Neurosciences, Bangalore 560029 Karnataka, India; Institute of Bioinformatics, International Technology Park, Bangalore 560066 Karnataka, India; Manipal Academy of Higher Education, Manipal 576104 Karnataka, India*

Kishore Garapati − *Department of Laboratory Medicine and Pathology, Mayo Clinic, Rochester, Minnesota 55905, United States; Institute of Bioinformatics, International Technology Park, Bangalore 560066 Karnataka, India; Manipal Academy of Higher Education, Manipal 576104 Karnataka, India*

Sandip Chavan − *Department of Laboratory Medicine and Pathology, Mayo Clinic, Rochester, Minnesota 55905, United States*

Jane A. Peterson − *Proteomics Core, Medical Genome Facility, Mayo Clinic, Rochester, Minnesota 55905, United States*

Mayank Saraswat − *Department of Laboratory Medicine and Pathology, Mayo Clinic, Rochester, Minnesota 55905, United States; Institute of Bioinformatics, International Technology Park, Bangalore 560066 Karnataka, India; Manipal Academy of Higher Education, Manipal 576104 Karnataka, India*

Complete contact information is available at: https://pubs.acs.org/10.1021/acs.jproteome.1c00506

Notes

The authors declare no competing financial interest.

■ ACKNOWLEDGMENTS

This study was supported by DBT/Wellcome Trust India Alliance Margdarshi Fellowship Grant IA/M/15/1/502023 awarded to Akhilesh Pandey and the generosity of Eric and Wendy Schmidt.

■ REFERENCES

(1) Ludwig, C.; Gillet, L.; Rosenberger, G.; Amon, S.; Collins, B. C.; Aebersold, R. Data-independent acquisition-based SWATH-MS for quantitative proteomics: a tutorial. *Mol. Syst. Biol.* **2018**, *14* (8), e8126.

(2) Zhang, F.; Ge, W.; Ruan, G.; Cai, X.; Guo, T. Data-Independent Acquisition Mass Spectrometry-Based Proteomics and Software Tools: A Glimpse in 2020. *Proteomics* **2020**, *20* (17−18), e1900276.

(3) Reubsaet, L.; Sweredoski, M. J.; Moradian, A. Data-Independent Acquisition for the Orbitrap Q Exactive HF: A Tutorial. *J. Proteome Res.* **2019**, *18* (3), 803−813.

(4) Chapman, J. D.; Goodlett, D. R.; Masselon, C. D. Multiplexed and data-independent tandem mass spectrometry for global proteome profiling. *Mass Spectrom. Rev.* **2014**, *33* (6), 452−70.

(5) Poulos, R. C.; Hains, P. G.; Shah, R.; Lucas, N.; Xavier, D.; Manda, S. S.; Anees, A.; Koh, J. M. S.; Mahboob, S.; Wittman, M.; Williams, S. G.; Sykes, E. K.; Hecker, M.; Dausmann, M.; Wouters, M. A.; Ashman, K.; Yang, J.; Wild, P. J.; deFazio, A.; Balleine, R. L.; Tully, B.; Aebersold, R.; Speed, T. P.; Liu, Y.; Reddel, R. R.; Robinson, P. J.; Zhong, Q. Strategies to enable large-scale proteomics for reproducible research. *Nat. Commun.* **2020**, *11* (1), 3793.

(6) Meier, F.; Brunner, A. D.; Frank, M.; Ha, A.; Bludau, I.; Voytik, E.; Kaspar-Schoenefeld, S.; Lubeck, M.; Raether, O.; Bache, N.; Aebersold, R.; Collins, B. C.; Rost, H. L.; Mann, M. diaPASEF: parallel accumulation-serial fragmentation combined with data-independent acquisition. *Nat. Methods* **2020**, *17* (12), 1229−1236.

(7) Huang, C.; Wang, Y.; Li, X.; Ren, L.; Zhao, J.; Hu, Y.; Zhang, L.; Fan, G.; Xu, J.; Gu, X.; Cheng, Z.; Yu, T.; Xia, J.; Wei, Y.; Wu, W.; Xie, X.; Yin, W.; Li, H.; Liu, M.; Xiao, Y.; Gao, H.; Guo, L.; Xie, J.; Wang, G.; Jiang, R.; Gao, Z.; Jin, Q.; Wang, J.; Cao, B. Clinical features of patients infected with 2019 novel coronavirus in Wuhan, China. *Lancet* **2020**, *395* (10223), 497−506.

(8) Blanco-Melo, D.; Nilsson-Payant, B. E.; Liu, W. C.; Uhl, S.; Hoagland, D.; Møller, R.; Jordan, T. X.; Oishi, K.; Panis, M.; Sachs, D.; Wang, T. T.; Schwartz, R. E.; Lim, J. K.; Albrecht, R. A.; tenOever, B. R. Imbalanced Host Response to SARS-CoV-2 Drives Development of COVID-19. *Cell* **2020**, *181* (5), 1036−1045.

(9) Zhou, Z.; Ren, L.; Zhang, L.; Zhong, J.; Xiao, Y.; Jia, Z.; Guo, L.; Yang, J.; Wang, C.; Jiang, S.; Yang, D.; Zhang, G.; Li, H.; Chen, F.; Xu, Y.; Chen, M.; Gao, Z.; Yang, J.; Dong, J.; Liu, B.; Zhang, X.; Wang, W.; He, K.; Jin, Q.; Li, M.; Wang, J. Heightened Innate Immune Responses in the Respiratory Tract of COVID-19 Patients. *Cell Host Microbe* **2020**, *27* (6), 883−890.

(10) Wu, M.; Chen, Y.; Xia, H.; Wang, C.; Tan, C. Y.; Cai, X.; Liu, Y.; Ji, F.; Xiong, P.; Liu, R.; Guan, Y.; Duan, Y.; Kuang, D.; Xu, S.; Cai, H.; Xia, Q.; Yang, D.; Wang, M. W.; Chiu, I. M.; Cheng, C.; Ahern, P. P.; Liu, L.; Wang, G.; Surana, N. K.; Xia, T.; Kasper, D. L. Transcriptional and proteomic insights into the host response in fatal COVID-19 cases. *Proc. Natl. Acad. Sci. U. S. A.* **2020**, *117* (45), 28336−28343.

(11) Chua, R. L.; Lukassen, S.; Trump, S.; Hennig, B. P.; Wendisch, D.; Pott, F.; Debnath, O.; Thurmann, L.; Kurth, F.; Volker, M. T.; Kazmierski, J.; Timmermann, B.; Twardziok, S.; Schneider, S.; Machleidt, F.; Muller-Redetzky, H.; Maier, M.; Krannich, A.; Schmidt, S.; Balzer, F.; Liebig, J.; Loske, J.; Suttorp, N.; Eils, J.; Ishaque, N.; Liebert, U. G.; von Kalle, C.; Hocke, A.; Witzenrath, M.; Goffinet, C.; Drosten, C.; Laudi, S.; Lehmann, I.; Conrad, C.; Sander, L. E.; Eils, R. COVID-19 severity correlates with airway epithelium-immune cell interactions identified by single-cell analysis. *Nat. Biotechnol.* **2020**, *38* (8), 970−979.

(12) Schmidt, N.; Lareau, C. A.; Keshishian, H.; Ganskih, S.; Schneider, C.; Hennig, T.; Melanson, R.; Werner, S.; Wei, Y.; Zimmer, M.; Ade, J.; Kirschner, L.; Zielinski, S.; Dolken, L.; Lander, E. S.; Caliskan, N.; Fischer, U.; Vogel, J.; Carr, S. A.; Bodem, J.; Munschauer, M. The SARS-CoV-2 RNA-protein interactome in infected human cells. *Nat. Microbiol* **2021**, *6* (3), 339−353.

(13) Bojkova, D.; Klann, K.; Koch, B.; Widera, M.; Krause, D.; Ciesek, S.; Cinatl, J.; Munch, C. Proteomics of SARS-CoV-2-infected host cells reveals therapy targets. *Nature* **2020**, *583* (7816), 469−472.

(14) Tushir, S.; Kamanna, S.; Nath, S. S.; Bhat, A.; Rose, S.; Aithal, A. R.; Tatu, U. Proteo-Genomic Analysis of SARS-CoV-2: A Clinical Landscape of Single-Nucleotide Polymorphisms, COVID-19 Proteome, and Host Responses. *J. Proteome Res.* **2021**, *20* (3), 1591−1601.

(15) Shen, B.; Yi, X.; Sun, Y.; Bi, X.; Du, J.; Zhang, C.; Quan, S.; Zhang, F.; Sun, R.; Qian, L.; Ge, W.; Liu, W.; Liang, S.; Chen, H.; Zhang, Y.; Li, J.; Xu, J.; He, Z.; Chen, B.; Wang, J.; Yan, H.; Zheng, Y.; Wang, D.; Zhu, J.; Kong, Z.; Kang, Z.; Liang, X.; Ding, X.; Ruan, G.; Xiang, N.; Cai, X.; Gao, H.; Li, L.; Li, S.; Xiao, Q.; Lu, T.; Zhu, Y.; Liu, H.; Chen, H.; Guo, T. Proteomic and Metabolomic Characterization of COVID-19 Patient Sera. *Cell* **2020**, *182* (1), 59−72.

(16) Overmyer, K. A.; Shishkova, E.; Miller, I. J.; Balnis, J.; Bernstein, M. N.; Peters-Clarke, T. M.; Meyer, J. G.; Quan, Q.;

Muehlbauer, L. K.; Trujillo, E. A.; He, Y.; Chopra, A.; Chieng, H. C.; Tiwari, A.; Judson, M. A.; Paulson, B.; Brademan, D. R.; Zhu, Y.; Serrano, L. R.; Linke, V.; Drake, L. A.; Adam, A. P.; Schwartz, B. S.; Singer, H. A.; Swanson, S.; Mosher, D. F.; Stewart, R.; Coon, J. J.; Jaitovich, A. Large-Scale Multi-omic Analysis of COVID-19 Severity. *Cell Syst* **2021**, *12* (1), 23−40.

(17) Gallo, O.; Locatello, L. G.; Mazzoni, A.; Novelli, L.; Annunziato, F. The central role of the nasal microenvironment in the transmission, modulation, and clinical progression of SARS-CoV-2 infection. *Mucosal Immunol.* **2021**, *14* (2), 305−316.

(18) Hewitt, R. J.; Lloyd, C. M. Regulation of immune responses by the airway epithelial cell landscape. *Nat. Rev. Immunol.* **2021**, *21* (6), 347−362.

(19) Hoffmann, M.; Kleine-Weber, H.; Schroeder, S.; Kruger, N.; Herrler, T.; Erichsen, S.; Schiergens, T. S.; Herrler, G.; Wu, N. H.; Nitsche, A.; Muller, M. A.; Drosten, C.; Pohlmann, S. SARS-CoV-2 Cell Entry Depends on ACE2 and TMPRSS2 and Is Blocked by a Clinically Proven Protease Inhibitor. *Cell* **2020**, *181* (2), 271−280.

(20) Haas, P.; Muralidharan, M.; Krogan, N. J.; Kaake, R. M.; Huttenhain, R. Proteomic Approaches to Study SARS-CoV-2 Biology and COVID-19 Pathology. *J. Proteome Res.* **2021**, *20* (2), 1133−1152.

(21) Nachtigall, F. M.; Pereira, A.; Trofymchuk, O. S.; Santos, L. S. Detection of SARS-CoV-2 in nasal swabs using MALDI-MS. *Nat. Biotechnol.* **2020**, *38* (10), 1168−1173.

(22) Gouveia, D.; Miotello, G.; Gallais, F.; Gaillard, J. C.; Debroas, S.; Bellanger, L.; Lavigne, J. P.; Sotto, A.; Grenga, L.; Pible, O.; Armengaud, J. Proteotyping SARS-CoV-2 Virus from Nasopharyngeal Swabs: A Proof-of-Concept Focused on a 3 min Mass Spectrometry Window. *J. Proteome Res.* **2020**, *19* (11), 4407−4416.

(23) Cardozo, K. H. M.; Lebkuchen, A.; Okai, G. G.; Schuch, R. A.; Viana, L. G.; Olive, A. N.; Lazari, C. D. S.; Fraga, A. M.; Granato, C. F. H.; Pintao, M. C. T.; Carvalho, V. M. Establishing a mass spectrometry-based system for rapid detection of SARS-CoV-2 in large clinical sample cohorts. *Nat. Commun.* **2020**, *11* (1), 6201.

(24) Szklarczyk, D.; Gable, A. L.; Lyon, D.; Junge, A.; Wyder, S.; Huerta-Cepas, J.; Simonovic, M.; Doncheva, N. T.; Morris, J. H.; Bork, P.; Jensen, L. J.; Mering, C. V. STRING v11: protein-protein association networks with increased coverage, supporting functional discovery in genome-wide experimental datasets. *Nucleic Acids Res.* **2019**, *47* (D1), D607−D613.

(25) Perez-Riverol, Y.; Csordas, A.; Bai, J.; Bernal-Llinares, M.; Hewapathirana, S.; Kundu, D. J.; Inuganti, A.; Griss, J.; Mayer, G.; Eisenacher, M.; Perez, E.; Uszkoreit, J.; Pfeuffer, J.; Sachsenberg, T.; Yilmaz, S.; Tiwary, S.; Cox, J.; Audain, E.; Walzer, M.; Jarnuczak, A. F.; Ternent, T.; Brazma, A.; Vizcaino, J. A. The PRIDE database and related tools and resources in 2019: improving support for quantification data. *Nucleic Acids Res.* **2019**, *47* (D1), D442−D450.

(26) Tabb, D. L.; Vega-Montoto, L.; Rudnick, P. A.; Variyath, A. M.; Ham, A. J.; Bunk, D. M.; Kilpatrick, L. E.; Billheimer, D. D.; Blackman, R. K.; Cardasis, H. L.; Carr, S. A.; Clauser, K. R.; Jaffe, J. D.; Kowalski, K. A.; Neubert, T. A.; Regnier, F. E.; Schilling, B.; Tegeler, T. J.; Wang, M.; Wang, P.; Whiteaker, J. R.; Zimmerman, L. J.; Fisher, S. J.; Gibson, B. W.; Kinsinger, C. R.; Mesri, M.; Rodriguez, H.; Stein, S. E.; Tempst, P.; Paulovich, A. G.; Liebler, D. C.; Spiegelman, C. Repeatability and reproducibility in proteomic identifications by liquid chromatography-tandem mass spectrometry. *J. Proteome Res.* **2010**, *9* (2), 761−76.

(27) Meier, F.; Brunner, A. D.; Koch, S.; Koch, H.; Lubeck, M.; Krause, M.; Goedecke, N.; Decker, J.; Kosinski, T.; Park, M. A.; Bache, N.; Hoerning, O.; Cox, J.; Rather, O.; Mann, M. Online Parallel Accumulation-Serial Fragmentation (PASEF) with a Novel Trapped Ion Mobility Mass Spectrometer. *Mol. Cell Proteomics* **2018**, *17* (12), 2534−2545.

(28) Meier, F.; Beck, S.; Grassl, N.; Lubeck, M.; Park, M. A.; Raether, O.; Mann, M. Parallel Accumulation-Serial Fragmentation (PASEF): Multiplying Sequencing Speed and Sensitivity by Synchronized Scans in a Trapped Ion Mobility Device. *J. Proteome Res.* **2015**, *14* (12), 5378−87.

(29) Renuse, S.; Vanderboom, P. M.; Maus, A. D.; Kemp, J. V.; Gurtner, K. M.; Madugundu, A. K.; Chavan, S.; Peterson, J. A.; Madden, B. J.; Mangalaparthi, K. K.; Mun, D.-G.; Singh, S.; Kipp, B. R.; Dasari, S.; Singh, R. J.; Grebe, S. K.; Pandey, A. A mass spectrometry-based targeted assay for detection of SARS-CoV-2 antigen from clinical specimens. *EBioMedicine* **2021**, *69*, 103465.

(30) Sande, C. J.; Njunge, J. M.; Mwongeli Ngoi, J.; Mutunga, M. N.; Chege, T.; Gicheru, E. T.; Gardiner, E. M.; Gwela, A.; Green, C. A.; Drysdale, S. B.; Berkley, J. A.; Nokes, D. J.; Pollard, A. J. Airway response to respiratory syncytial virus has incidental antibacterial effects. *Nat. Commun.* **2019**, *10* (1), 2218.

(31) Ndika, J.; Airaksinen, L.; Suojalehto, H.; Karisola, P.; Fyhrquist, N.; Puustinen, A.; Alenius, H. Epithelial proteome profiling suggests the essential role of interferon-inducible proteins in patients with allergic rhinitis. *J. Allergy Clin. Immunol.* **2017**, *140* (5), 1288−1298.

(32) Kuleshov, M. V.; Jones, M. R.; Rouillard, A. D.; Fernandez, N. F.; Duan, Q.; Wang, Z.; Koplev, S.; Jenkins, S. L.; Jagodnik, K. M.; Lachmann, A.; McDermott, M. G.; Monteiro, C. D.; Gundersen, G. W.; Ma'ayan, A. Enrichr: a comprehensive gene set enrichment analysis web server 2016 update. *Nucleic Acids Res.* **2016**, *44* (W1), W90−7.

(33) Schwanhausser, B.; Busse, D.; Li, N.; Dittmar, G.; Schuchhardt, J.; Wolf, J.; Chen, W.; Selbach, M. Global quantification of mammalian gene expression control. *Nature* **2011**, *473* (7347), 337−42.

(34) Zahn-Zabal, M.; Michel, P. A.; Gateau, A.; Nikitin, F.; Schaeffer, M.; Audot, E.; Gaudet, P.; Duek, P. D.; Teixeira, D.; Rech de Laval, V.; Samarasinghe, K.; Bairoch, A.; Lane, L. The neXtProt knowledgebase in 2020: data, tools and usability improvements. *Nucleic Acids Res.* **2020**, *48* (D1), D328−D334.

(35) Assarsson, E.; Lundberg, M.; Holmquist, G.; Bjorkesten, J.; Bucht Thorsen, S.; Ekman, D.; Eriksson, A.; Rennel Dickens, E.; Ohlsson, S.; Edfeldt, G.; Andersson, A.-C.; Lindstedt, P.; Stenvang, J.; Gullberg, M.; Fredriksson, S. Homogenous 96-plex PEA immunoassay exhibiting high sensitivity, specificity, and excellent scalability. *PLoS One* **2014**, *9* (4), e95192.

(36) Rusinova, I.; Forster, S.; Yu, S.; Kannan, A.; Masse, M.; Cumming, H.; Chapman, R.; Hertzog, P. J. Interferome v2.0: an updated database of annotated interferon-regulated genes. *Nucleic Acids Res.* **2012**, *41*, D1040.

(37) Guo, Q.; Zhao, Y.; Li, J.; Liu, J.; Yang, X.; Guo, X.; Kuang, M.; Xia, H.; Zhang, Z.; Cao, L.; Luo, Y.; Bao, L.; Wang, X.; Wei, X.; Deng, W.; Wang, N.; Chen, L.; Chen, J.; Zhu, H.; Gao, R.; Qin, C.; Wang, X.; You, F. Induction of alarmin S100A8/A9 mediates activation of aberrant neutrophils in the pathogenesis of COVID-19. *Cell Host Microbe* **2021**, *29* (2), 222−235.

(38) Weidberg, H.; Elazar, Z. TBK1 mediates crosstalk between the innate immune response and autophagy. *Sci. Signaling* **2011**, *4* (187), pe39.

(39) Zhou, R.; Zhang, Q.; Xu, P. TBK1, a central kinase in innate immune sensing of nucleic acids and beyond. *Acta Biochim Biophys Sin (Shanghai)* **2020**, *52* (7), 757−767.

(40) Xia, H.; Cao, Z.; Xie, X.; Zhang, X.; Chen, J. Y.; Wang, H.; Menachery, V. D.; Rajsbaum, R.; Shi, P. Y. Evasion of Type I Interferon by SARS-CoV-2. *Cell Rep.* **2020**, *33* (1), 108234.

(41) Lei, X.; Dong, X.; Ma, R.; Wang, W.; Xiao, X.; Tian, Z.; Wang, C.; Wang, Y.; Li, L.; Ren, L.; Guo, F.; Zhao, Z.; Zhou, Z.; Xiang, Z.; Wang, J. Activation and evasion of type I interferon responses by SARS-CoV-2. *Nat. Commun.* **2020**, *11* (1), 3810.

(42) El-Diwany, R.; Soliman, M.; Sugawara, S.; Breitwieser, F.; Skaist, A.; Coggiano, C.; Sangal, N.; Chattergoon, M.; Bailey, J. R.; Siliciano, R. F.; Blankson, J. N.; Ray, S. C.; Wheelan, S. J.; Thomas, D. L.; Balagopal, A. CMPK2 and BCL-G are associated with type 1 interferon-induced HIV restriction in humans. *Sci. Adv.* **2018**, *4* (8), eaat0843.

(43) Huang, D. W.; Sherman, B. T; Lempicki, R. A Systematic and integrative analysis of large gene lists using DAVID bioinformatics resources. *Nat. Protoc.* **2009**, *4* (1), 44−57.

https://doi.org/10.1021/acs.jproteome.1c00506
J. Proteome Res. XXXX, XXX, XXX−XXX

(44) Bingle, L.; Cross, S. S.; High, A. S.; Wallace, W. A.; Rassl, D.; Yuan, G.; Hellstrom, I.; Campos, M. A.; Bingle, C. D. WFDC2 (HE4): a potential role in the innate immunity of the oral cavity and respiratory tract and the development of adenocarcinomas of the lung. *Respir. Res.* **2006**, *7*, 61.
(45) Bonser, L. R.; Schroeder, B. W.; Ostrin, L. A.; Baumlin, N.; Olson, J. L.; Salathe, M.; Erle, D. J. The Endoplasmic Reticulum Resident Protein AGR3. Required for Regulation of Ciliary Beat Frequency in the Airway. *Am. J. Respir. Cell Mol. Biol.* **2015**, *53* (4), 536−43.
(46) Reikine, S.; Nguyen, J. B.; Modis, Y. Pattern Recognition and Signaling Mechanisms of RIG-I and MDA5. *Front. Immunol.* **2014**, *5*, 342.
(47) Chavan, S.; Mangalaparthi, K. K.; Singh, S.; Renuse, S.; Vanderboom, P. M.; Madugundu, A. K.; Budhraja, R.; McAulay, K.; Grys, T. E.; Rule, A. D.; Alexander, M. P.; O'Horo, J. C.; Badley, A. D.; Pandey, A. Mass Spectrometric Analysis of Urine from COVID-19 Patients for Detection of SARS-CoV-2 Viral Antigen and to Study Host Response. *J. Proteome Res.* **2021**, *20*, 3404.
(48) Mostafavi, S.; Yoshida, H.; Moodley, D.; LeBoite, H.; Rothamel, K.; Raj, T.; Ye, C. J.; Chevrier, N.; Zhang, S. Y.; Feng, T.; Lee, M.; Casanova, J. L.; Clark, J. D.; Hegen, M.; Telliez, J. B.; Hacohen, N.; De Jager, P. L.; Regev, A.; Mathis, D.; Benoist, C. Parsing the Interferon Transcriptional Network and Its Disease Associations. *Cell* **2016**, *164* (3), 564−578.
(49) Li, L.; Zhao, H.; Liu, P.; Li, C.; Quanquin, N.; Ji, X.; Sun, N.; Du, P.; Qin, C. F.; Lu, N.; Cheng, G. PARP12 suppresses Zika virus infection through PARP-dependent degradation of NS1 and NS3 viral proteins. *Sci. Signaling* **2018**, *11* (535), eaas9332.
(50) Mifflin, L.; Ofengeim, D.; Yuan, J. Receptor-interacting protein kinase 1 (RIPK1) as a therapeutic target. *Nat. Rev. Drug Discovery* **2020**, *19* (8), 553−571.
(51) Dunkelberger, J. R.; Song, W. C. Complement and its role in innate and adaptive immune responses. *Cell Res.* **2010**, *20* (1), 34−50.
(52) Holter, J. C.; Pischke, S. E.; de Boer, E.; Lind, A.; Jenum, S.; Holten, A. R.; Tonby, K.; Barratt-Due, A.; Sokolova, M.; Schjalm, C.; Chaban, V.; Kolderup, A.; Tran, T.; Tollefsrud Gjolberg, T.; Skeie, L. G.; Hesstvedt, L.; Ormasen, V.; Fevang, B.; Austad, C.; Muller, K. E.; Fladeby, C.; Holberg-Petersen, M.; Halvorsen, B.; Muller, F.; Aukrust, P.; Dudman, S.; Ueland, T.; Andersen, J. T.; Lund-Johansen, F.; Heggelund, L.; Dyrhol-Riise, A. M.; Mollnes, T. E. Systemic complement activation is associated with respiratory failure in COVID-19 hospitalized patients. *Proc. Natl. Acad. Sci. U. S. A.* **2020**, *117* (40), 25018−25025.
(53) Risco, C.; Rodriguez, J. R.; Lopez-Iglesias, C.; Carrascosa, J. L.; Esteban, M.; Rodriguez, D. Endoplasmic reticulum-Golgi intermediate compartment membranes and vimentin filaments participate in vaccinia virus assembly. *J. Virol.* **2002**, *76* (4), 1839−55.
(54) Sicari, D.; Chatziioannou, A.; Koutsandreas, T.; Sitia, R.; Chevet, E. Role of the early secretory pathway in SARS-CoV-2 infection. *J. Cell Biol.* **2020**, *219* (9), e202006005.
(55) Klaus, J. P.; Eisenhauer, P.; Russo, J.; Mason, A. B.; Do, D.; King, B.; Taatjes, D.; Cornillez-Ty, C.; Boyson, J. E.; Thali, M.; Zheng, C.; Liao, L.; Yates, J. R., 3rd; Zhang, B.; Ballif, B. A.; Botten, J. W. The intracellular cargo receptor ERGIC-53 is required for the production of infectious arenavirus, coronavirus, and filovirus particles. *Cell Host Microbe* **2013**, *14* (5), 522−34.
(56) Realegeno, S.; Priyamvada, L.; Kumar, A.; Blackburn, J. B.; Hartloge, C.; Puschnik, A. S.; Sambhara, S.; Olson, V. A.; Carette, J. E.; Lupashin, V.; Satheshkumar, P. S. Conserved Oligomeric Golgi (COG) Complex Proteins Facilitate Orthopoxvirus Entry, Fusion and Spread. *Viruses* **2020**, *12* (7), 707.
(57) Cheung, A.; Bax, H. J.; Josephs, D. H.; Ilieva, K. M.; Pellizzari, G.; Opzoomer, J.; Bloomfield, J.; Fittall, M.; Grigoriadis, A.; Figini, M.; Canevari, S.; Spicer, J. F.; Tutt, A. N.; Karagiannis, S. N. Targeting folate receptor alpha for cancer treatment. *Oncotarget* **2016**, *7* (32), 52553−52574.
(58) Gordon, D. E.; Jang, G. M.; Bouhaddou, M.; Xu, J.; Obernier, K.; White, K. M.; O'Meara, M. J.; Rezelj, V. V.; Guo, J. Z.; Swaney, D. L.; Tummino, T. A.; Huttenhain, R.; Kaake, R. M.; Richards, A. L.; Tutuncuoglu, B.; Foussard, H.; Batra, J.; Haas, K.; Modak, M.; Kim, M.; Haas, P.; Polacco, B. J.; Braberg, H.; Fabius, J. M.; Eckhardt, M.; Soucheray, M.; Bennett, M. J.; Cakir, M.; McGregor, M. J.; Li, Q.; Meyer, B.; Roesch, F.; Vallet, T.; Mac Kain, A.; Miorin, L.; Moreno, E.; Naing, Z. Z. C.; Zhou, Y.; Peng, S.; Shi, Y.; Zhang, Z.; Shen, W.; Kirby, I. T.; Melnyk, J. E.; Chorba, J. S.; Lou, K.; Dai, S. A.; Barrio-Hernandez, I.; Memon, D.; Hernandez-Armenta, C.; Lyu, J.; Mathy, C. J. P.; Perica, T.; Pilla, K. B.; Ganesan, S. J.; Saltzberg, D. J.; Rakesh, R.; Liu, X.; Rosenthal, S. B.; Calviello, L.; Venkataramanan, S.; Liboy-Lugo, J.; Lin, Y.; Huang, X. P.; Liu, Y.; Wankowicz, S. A.; Bohn, M.; Safari, M.; Ugur, F. S.; Koh, C.; Savar, N. S.; Tran, Q. D.; Shengjuler, D.; Fletcher, S. J.; O'Neal, M. C.; Cai, Y.; Chang, J. C. J.; Broadhurst, D. J.; Klippsten, S.; Sharp, P. P.; Wenzell, N. A.; Kuzuoglu-Ozturk, D.; Wang, H. Y.; Trenker, R.; Young, J. M.; Cavero, D. A.; Hiatt, J.; Roth, T. L.; Rathore, U.; Subramanian, A.; Noack, J.; Hubert, M.; Stroud, R. M.; Frankel, A. D.; Rosenberg, O. S.; Verba, K. A.; Agard, D. A.; Ott, M.; Emerman, M.; Jura, N.; von Zastrow, M.; Verdin, E.; Ashworth, A.; Schwartz, O.; d'Enfert, C.; Mukherjee, S.; Jacobson, M.; Malik, H. S.; Fujimori, D. G.; Ideker, T.; Craik, C. S.; Floor, S. N.; Fraser, J. S.; Gross, J. D.; Sali, A.; Roth, B. L.; Ruggero, D.; Taunton, J.; Kortemme, T.; Beltrao, P.; Vignuzzi, M.; Garcia-Sastre, A.; Shokat, K. M.; Shoichet, B. K.; Krogan, N. J. A SARS-CoV-2 protein interaction map reveals targets for drug repurposing. *Nature* **2020**, *583* (7816), 459−468.

https://doi.org/10.1021/acs.jproteome.1c00506
J. Proteome Res. XXXX, XXX, XXX−XXX